Internal Geophysics (Physics of Earth's Interior)

Density variations of Cr-rich garnets in the upper mantle inferred from the elasticity of uvarovite garnet

Steeve Gréaux [a,b,*], Akihiro Yamada [a,1]

[a] *Geodynamics Research Center, Ehime University, 790-8577 Matsuyama, Japan*
[b] *Earth-Life Science Institute, Tokyo Institute of Technology, 152-8550 Tokyo, Japan*

ARTICLE INFO

ABSTRACT

The thermoelastic parameters of $Ca_3Cr_2Si_3O_{12}$ uvarovite garnet were examined *in situ* at high pressure up to 13 GPa and high temperature up to 1100 K by synchrotron radiation energy-dispersive X-ray diffraction within a 6-6-type multi-anvil press apparatus. A least-square fitting of room T data to a third-order Birch–Murnaghan (BM3) EoS yielded K_0 = 164.2 ± 0.7 GPa, V_0 = 1735.9 ± 0.3 Å^3 (K'_0 fixed to 4.0). P–V–T data were fitted simultaneously by a modified HT-BM3 EoS, which gave the isothermal bulk modulus K_0 = 163.6 ± 2.6 GPa, K'_0 = 4.1 ± 0.5, its temperature derivative $(\partial K_{0,T}/\partial T)_P$ = −0.014 ± 0.002 GPa K^{-1}, and the thermal expansion coefficients a_0 = 2.32 ± 0.13 ×10^{-5} K^{-1} and b_0 = 2.13 ± 2.18 ×10^{-9} K^{-2} (K'_0 fixed to 4.0). Our results showed that the Cr^{3+} enrichment in natural systems likely increases the density of ugrandite garnets, resulting in a substantial increase of mantle garnet densities in regions where Cr-rich spinel releases chromium through a metasomatic reaction.

© 2018 Académie des sciences. Published by Elsevier Masson SAS. All rights reserved.

1. Introduction

Silicate garnets constitute a large family of rock-forming minerals that are considered to be a major constituent of the Earth's upper mantle (Bass and Anderson, 1984; Green and Ringwood, 1967). Among mantle garnets, Cr-rich garnets are less common minerals that form in mafic and ultramafic rocks that have undergone metasomatic reactions at relatively low temperature and pressure (Challis et al., 1995; Mogessie and Rammlmair, 1994; Proenza et al., 1999). However, geological and petrological studies have demonstrated that the chromium concentration in garnet increases with depth, along with the spinel-garnet transformation up to 7 GPa (Klemme, 2004), which has important implications for the geobarometry of rock samples returned from the deep mantle (Grutter et al., 2006). Despite constituting a minor fraction of mantle garnets, Cr-garnet might become more important at the bottom of the upper mantle when Cr-rich spinel decomposes through metasomatic reactions. Therefore, knowledge of the elasticity of Cr-garnet is important to estimate the effect of Cr^{3+} incorporation on the physical properties of mantle garnets and its possible implications for the interpretation of deep-Earth structures.

Mantle garnets form complex non-ideal solid solutions, whose physical properties may change as a function of pressure, temperature and chemical composition. The structure of silicate garnets $X_3^{2+}Y_2^{3+}Si_3O_{12}$ consists of a mixed framework of corner-sharing SiO_4 tetrahedra and YO_6 octahedra, with twisted XO_8 cubes lying in between. In natural garnet the X-site is exclusively occupied by

---

* Corresponding author at: Geodynamics Research Center, Ehime University, 790-8577 Matsuyama, Japan.

E-mail address: greaux@sci.ehime-u.ac.jp (S. Gréaux).

[1] Now at the University of Shiga prefecture, 2500 Hassaka, Hikone, 522-8533 Shiga, Japan.

divalent cations (Mg^{2+}, Fe^{2+}, Ca^{2+}, Mn^{2+}), whereas the Y-site normally hosts trivalent cations (Al^{3+}, Fe^{3+}, Cr^{3+}) (Deer et al., 1962). The variety of the garnet chemistry makes it difficult to establish a relation between chemical composition and elasticity by a direct study at high pressure and temperature. For this reason, previous studies have been investigating the elasticity of garnet endmembers at high P and T (among many others, Bass, 1989; Conrad et al., 1999; Gréaux and Yamada, 2013; Gréaux et al., 2010; Pavese et al., 2001; Sinogeikin and Bass, 2002; Zou et al., 2012b), from which they derived the elasticity of more complex solid solutions.

In the Earth's mantle, $Ca_3Cr_2Si_3O_{12}$ uvarovite and $Mg_3Cr_2Si_3O_{12}$ knorringite are of the most relevant Cr-garnet endmembers and are commonly found in xenoliths and inclusions in diamonds from the deep mantle (Deer et al., 1962; Irifune et al., 1982; Klemme, 2004). Uvarovite garnet was reported to be stable in a wide range of pressures and temperatures, and hence is found in various metamorphic rocks in the form of aggregates of tiny crystals that usually contain significant amounts of grossular and andradite (Deer et al., 1962). On the other hand, phase relation and stability of knorringite, despite remaining controversial (Klemme, 2004; Zou and Irifune, 2012), suggested that this endmember may not be stable in upper mantle conditions. Therefore, uvarovite garnet might be the most relevant Cr-garnet endmember to investigate the effect of Cr^{3+} incorporation on the physical properties of silicate garnets in upper mantle conditions.

The elasticity of uvarovite garnet was formerly studied by Brillouin spectroscopy on single crystals at room conditions (see Bass, 1986, and references therein). Subsequently, experiments at high pressure and room temperature were conducted to investigate the elasticity of natural and synthetic uvarovite specimens (Bass, 1986; Diella et al., 2004; Léger et al., 1990>). Léger et al. (1990) reported the isothermal compressibility of a polycrystalline aggregate at 300 K by using a diamond anvil cell (DAC) and proposed the first pressure derivative $K' = 4.7$ assuming the bulk modulus $K_0 = 162$ GPa given by Bass (1986). More recent experiments on the basis of *in situ* X-ray measurements in a laser-heated diamond anvil cell up to 16.2 GPa and 900 K (Fan et al., 2015) reported $K_0 = 162$ GPa and $K' = 4.0$–4.5 and the thermal expansion $\alpha_0 = 2.72 \times 10^{-5}$ K^{-1}, which is slightly larger than $\alpha_0 = 2.15 \times 10^{-5}$ K^{-1} proposed by lattice energy and vibrational energy calculations (Ottonello et al., 1996).

Here we investigated the pressure–volume–temperature relation of a synthetic uvarovite garnet $Ca_3Cr_2Si_3O_{12}$ up to 12.7 GPa and 1100 K using a multi-anvil apparatus combined with synchrotron Energy-Dispersive X-Ray Diffraction (EDXRD) measurements at the beamline AR-NE5 C (KEK-Photon Factory, Japan). The use of a large-volume apparatus allowed for precise control of pressure and temperature, while energy-dispersive X-ray diffraction (EDXRD) measurements were carried out *in situ* at high pressures and temperatures up to 12.7 GPa and 1100 K. Thermoelastic properties of uvarovite garnet were derived using the high-temperature equation of state (EoS). Results are discussed relative to other garnet endmembers and garnet solid solutions to estimate the

effect of Cr^{3+} on the density of mantle garnets in P and T conditions of the upper mantle.

2. Material and methods

Starting materials were prepared as a mechanical mixture of reagent-grade oxides in the molar proportions: $3CaCO_3 \cdot 1Cr_2O_3 \cdot 3SiO_2$. The mixture was placed ~20 h at 1173 K to remove carbonate and then hot-pressed at ~7 GPa and 1673 K for 2 h using a Kawai-type multi-anvil press apparatus ORANGE2000 at the Geodynamics Research Center (Ehime University, Matsuyama, Japan). The recovered sample was sintered and consisted mainly of uvarovite garnet, with minor amounts of Cr_2O_3 and CaO from the starting material. The chemical composition of the uvarovite garnet was analyzed by a Field-Emission Scanning Electron Microscope (FE-SEM) equipped with an Energy-Dispersive X-ray Spectrometer (EDS), which yielded the composition (in wt% with standard deviation in parentheses): CaO, 33.8(1); Cr_2O_3, 30.9(1); SiO_2, 35.5(1); i.e. $Ca_{3.02}Cr_{2.04}Si_{2.96}O_{12}$ on the basis of 12 oxygens. Micro-focused X-ray diffraction analysis of the sample yielded $a_0 = 12.002 \pm 0.002$ Å, which is compatible with previous reports that scatter within 11.988–12.010 Å (Andrut and Wildner, 2002; Bass, 1986; Léger et al., 1990; Novak and Gibbs, 1971).

High-pressure and high-temperature *in situ* experiments were carried out in a DIA-type multi-anvil press apparatus, MAX-80, located at the beamline AR-NE5 C of KEK-Photon Factory (Tsukuba Pref., Japan). High pressure was generated within what is called a 6-6-type cell assembly (Nishiyama et al., 2008) adapted for 4.0-mm truncation edge-length tungsten carbide anvils. The cell assembly consisted of a boron epoxy cubic pressure medium with a side length of 7.0 mm, a cylindrical graphite heater contained in a ZrO_2 insulator (Fig. 1), to reduce temperature gradients in the cell assembly. Pressure was estimated using the equation of state (EoS) of gold (Tsuchiya, 2003), which was mixed with MgO at a ratio of 10:1 (in wt.%) and placed near the hot junction of a $W_{97}Re_3$-$W_{75}Re_{25}$ thermocouple that was used to monitor temperature. The sample and pressure marker were surrounded by MgO to ensure a pseudo hydrostatic environment.
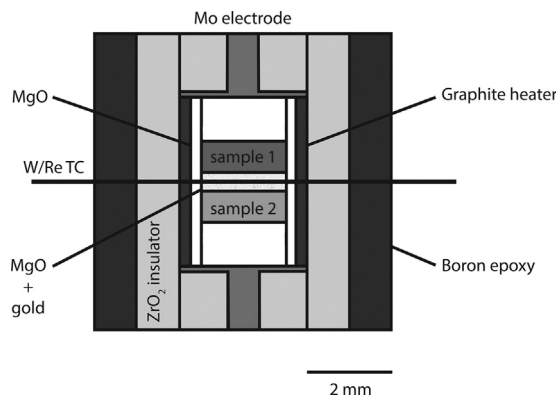

Fig. 1. Experimental cell assembly.

First, the sample is pressurized to 5.1 GPa and heated to 900 K. Temperature was maintained at 900 K for about 30 min to reduce non-hydrostatic stresses that can develop during cold compression. EDXRD measurements were carried out upon decrease of temperature to 300 K in steps of 200 K. All measurements in a given cooling cycle were done over a total duration of about 1 h. The heating/ collecting data procedure was repeated after each increment of pressure to 5.8, 7.8, 11.5, and 12.7 GPa, respectively. Further details about the procedures of the high-pressure and high-temperature measurements can be found in Gréaux and Yamada (2013).

All EDXRD patterns were collected at a fixed diffraction angle of ~6 degrees, which was calibrated on the basis of the diffraction pattern of gold at zero pressure; this method yielded an estimated error of 0.08 GPa in room conditions. Analyses of all XRD patterns were carried out by means of multi-peak fitting technique as implemented in the PDIndexer software package (Seto et al., 2010). XRD patterns of the pressure marker at high P and T were collected in between the hot-junction of the thermocouple and the sample (Fig. 1), while XRD patterns of the sample were collected at the closest location to the sample/ pressure marker interface. The temperature gradient between the thermocouple hot-junction and the sample was estimated to be about ± 25 K at 500 K and ± 40 K at 1100 K, on the basis of the two EoS of gold (Tsuchiya, 2003) and MgO (Tange et al., 2009) in the pressure marker. The precision upon the pressure was estimated from the uncertainties on the unit-cell volume of gold propagated to the pressure through the EoS of gold (Tsuchiya, 2003). The unit-cell volume of the uvarovite garnet and the corresponding pressure (Au-scale) and temperature are given in Table 1.

Fig. 2 shows the analysis results of the recovered sample. The ambient condition XRD profile is mainly explained by the diffraction peaks of the uvarovite garnet with minor peaks corresponding to excess Cr_2O_3 eskolaite, CaO lime from the starting material and two unidentified peaks (Fig. 2a). The FE-SEM observations of the recovered sample shows uvarovite garnet and minor amounts of Cr_2O_3 and CaO (Fig. 2b). No other phase was found in the sample. SEM-EDS analysis of the recovered sample yielded the composition CaO, 33.7(2); Cr_2O_3, 30.6(4); SiO_2, 35.7(2); i.e. $Ca_{3.01}Cr_{2.02}Si_{2.98}O_{12}$, which is close to the composition

of the starting material, suggesting that no reaction occurred between the garnet sample and surrounding materials during P–V–T measurements.

3. Results and discussion

3.1. Pressure–volume data at room temperature

The volume–pressure data relations have been determined by a least-square fitting of room-T data (Table 1) to the third-order Birch–Murnaghan (BM) equation of state whose general form is as follows:

$$P(V) = \frac{3}{2}K_0 \times \left[\left(\frac{V_0}{V}\right)^{\frac{7}{3}} - \left(\frac{V_0}{V}\right)^{\frac{5}{3}} \right] \times \left\{ 1 - \frac{3}{4}\left(4 - K'_0\right) \times \left[\left(\frac{V_0}{V}\right)^{\frac{2}{3}} - 1 \right] \right\}$$

(1)

where K_0, K'_0, and V_0 are the isothermal bulk modulus, its pressure derivative, and the zero-pressure unit-cell volume, respectively. Fitting of all parameters simultaneously using 300-K data collected at the end of each heating cycle, however, yielded large uncertainties ($K_0 = 166.2 \pm 2.4$ GPa, $K'_0 = 3.6 \pm 0.4$, and $V_0 = 1735.7 \pm 0.3$ Å^3), suggesting that all parameters cannot be resolved simultaneously due to the limited pressure range in this study. Therefore, we chose to fix the pressure derivative K'_0 at 4 here, which is compatible with the slightly positive slope of the normalized pressure against the Eulerian strain (inset of Fig. 3) that indicates a value of $K'_0 \geq 4$ (Angel, 2000). Fitting of equation (1) with K'_0 fixed at 4 yielded the bulk modulus $K_0 = 164.2 \pm 0.7$ GPa, which is in excellent agreement with $K_0 = 164 \pm 1$ GPa ($K'_0 = 4$) proposed by Fan et al. (2015) on the basis of angle-dispersive XRD in the diamond-anvil cell. Another fitting of equation (1) with K'_0 fixed at 4.5 gave $K_0 = 161.6 \pm 0.9$ GPa ($V_0 = 1736.1 \pm 0.3$ Å^3), which is also in good agreement with $K_0 = 162 \pm 2$ GPa, $K'_0 = 4.5 \pm 0.3$ derived by Fan et al. (2015) when they refined all parameters simultaneously (Table 2). The agreement on the results of elastic parameters and the small offset between data sets (Fig. 3), despite using two different techniques, suggests limited experimental uncertainties in our study and that of Fan et al. (2015).

When we fixed K'_0 at 4.7, we obtained a smaller $K_0 = 160.6 \pm 1.0$ GPa, which, within the uncertainties, is also in agreement with the values of $K_0 = 162$ and

Table 1
Experimental pressure, temperature and volume of uvarovite garnet.

Pressure (GPa)	Temperature (K)	Volume (Å^3)	Pressure (GPa)	Temperature (K)	Volume (Å^3)
0[a]	300	1735.8(1)	7.32(4)	700	1680.0(5)
5.44(5)	900	1704.6(15)	6.97(4)	500	1675.1(6)
4.89(5)	700	1703.3(12)	6.70(4)	300	1672.0(8)
4.43(5)	500	1699.7(11)	11.55(4)	1100	1656.6(7)
4.27(5)	300	1693.7(8)	10.97(4)	900	1655.4(7)
6.50(5)	900	1694.3(8)	10.53(4)	700	1652.3(9)
5.95(4)	700	1692.0(8)	10.08(4)	500	1649.6(8)
5.49(4)	500	1689.1(8)	9.86(4)	300	1635.9(7)
5.12(5)	300	1685.3(10)	13.08(5)	1100	1644.5(6)
8.43(4)	1100	1684.1(9)	10.97(6)	300	1635.9(7)
7.81(4)	900	1682.7(8)	0.94(3)	300	1726.0(2)

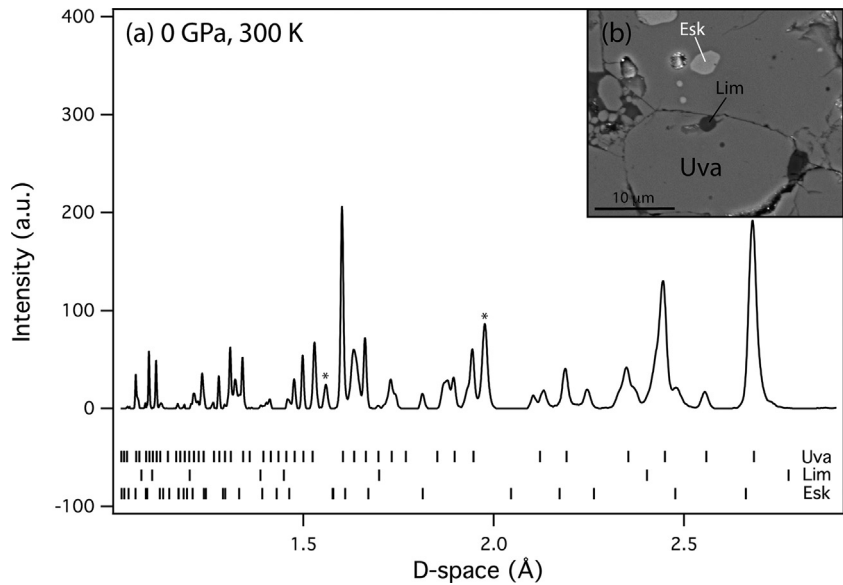[a] XRD pattern collected before compression.

Fig. 2. X-ray diffraction (XRD) pattern and scanning electron microscope (SEM) backscattered electron image of the recovered uvarovite sample. The XRD pattern could be explained by uvarovite garnet (Uva), eskolaite (Esk), lime (Lim) and two unidentified peaks **(a)**. SEM observations of the sample showed mainly uvarovite garnet with minor amounts of Cr_2O_3 (Esk) and CaO (Lim) from the starting material **(b)**. No other phase was found in the sample.

$K'_0 = 4.7$ proposed by Léger et al. (1990). Our results show that it is difficult to determine a unique K_0/K'_0 tradeoff for uvarovite garnet. This can be explained by the lack of constraints on the first pressure derivative K'_0, which is partly
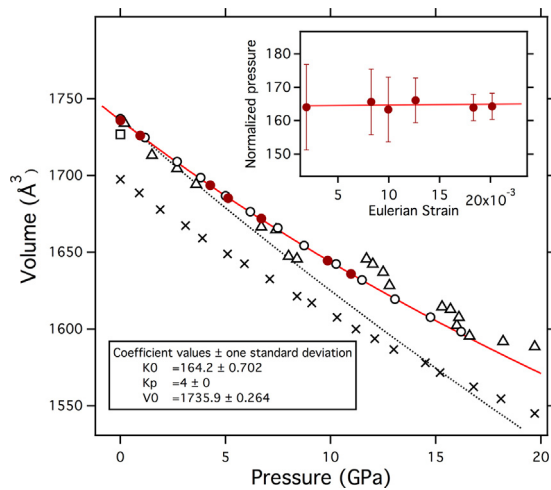

Fig. 3. Pressure–volume data of uvarovite garnet obtained in this study (plain circle), compared with the former experimental studies of Léger et al. (2000, open triangles) and Fan et al. (2015, open circle), while the broken line represents the uvarovite compression curve derived from theoretical calculations (Milman et al., 2001). Cross symbols represent data obtained by Diella et al. (2004) for a natural uvarovite-grossular garnet. Fitting of our P–V data (solid line) by a third-order Birch–Murnaghan equation of state fit yielded $K_{0,300} = 165.0 \pm 2.6$ GPa, $K'_{0,300} = 4.0 \pm 0.4$ and $V_{0,300} = 1735.8 \pm 0.4$ Å³. Error bars on the pressure and volume measurements are within the size of the symbols. Inset in the figure shows the normalized pressure versus the Eulerian strain plot based on the Birch–Murnaghan EoS at 300 K, where the solid line represents the linear fit through the data.

due to the limited pressure range addressed in all studies, respectively. One alternative way to determine the most appropriate set of moduli and derivatives would be to fit all available data simultaneously. We noted, however, that although below 10 GPa, the original P–V data of Léger et al. (1990) agree well with our data (Fig. 3), volumes at P higher than 10 GPa are larger, which is likely caused by anisotropic stress above 10 GPa due to the solidification of their methanol/ethanol pressure-transmitting medium (Léger et al., 1990), and therefore we excluded those data from the global fitting. The resulting elastic parameters $K_0 = 162.1 \pm 1.9$ GPa, $K'_0 = 4.3 \pm 0.3$ and $V_0 = 1736.5 \pm 0.4$ Å³ agree well, within uncertainties, with our data and those of Fan et al. (2015).

Table 2
Elasticity of uvarovite at 300 K.

$K_{0,300}$ (GPa)	$K'_{0,300}$	$V_{0,300}$ (Å³)	Reference	Methods
166.2 (24)	3.6 (4)	1735.7 (3)	This study	XRD-LVP
164.2 (7)	4.0[a]	1735.9 (3)		
161.6 (9)	4.5[a]	1736.1 (3)		
160.6 (10)	4.7[a]	1736.2 (4)		
162.1 (19)	4.3 (3)	1736.5 (4)	This study + Fan et al. (2015)	
162 (2)	–	1726.7	Bass (1986)	BS
162[a]	4.7 (7)	1732.3[a]	Leger et al. (1990)	XRD-DAC
160 (1)	5.8 (1)	1697.5	Diella et al. (2004)	XRD-DAC
164.8 (22)	4.7 (9)	1731.5	Wang and Ji (2001)	US-PC
143	4.7	1737.1	Milman et al. (2001)	Ab initio Calc.
164 (1)	4.0[a]	1736.5 (3)	Fan et al. (2015)	XRD-DAC
162 (2)	4.5 (3)	1736.9 (5)		

XRD: X-Ray Diffraction; LVP: Large Volume Press; DAC: Diamond Anvil Cell; BS: Brillouin Scattering; US: Ultrasonic interferometry; PC: piston cylinder apparatus; Calc.: *Ab Initio* calculation.
[a] Fixed during fitting.

It is worth noting that none of the parameters fitted here can explain the correlation between bulk modulus and its pressure derivatives for natural uvarovite samples (Diella et al., 2004; Wang and Ji, 2001), suggesting the Cr^{3+}/Al^{3+} ratio would have a substantial effect on the compressibility of those silicate garnets, which will be discussed a few sections below. Moreover, we cannot explain the low bulk modulus $K_0 = 143 \pm 4$ GPa for $K'_0 = 4.7$ proposed by Milman et al. (2001) based on an *ab initio* calculation by the density functional theory within the generalized gradient approximation. It is, however, difficult to draw any conclusion, because their calculations did not take into account the possibility of a Jahn–Teller effect that is expected to affect the compressibility of minerals containing octahedrally coordinated transition metals (Bass and Weidner, 1984; Pacalo et al., 1992; Zhang et al., 1998).

3.2. P–V–T data and thermoelastic parameters

Fitting of the pressure–volume–temperature data was carried out by a modified third-order Birch–Murnagham equation of state with the following form:

$$P(V,T) = \frac{3}{2} K_{0,T} \times \left[\left(\frac{V_{0,T}}{V_{P,T}} \right)^{\frac{7}{3}} - \left(\frac{V_{0,T}}{V_{P,T}} \right)^{\frac{5}{3}} \right]$$
$$\times \left\{ 1 - \frac{3}{4} \left(4 - K'_0 \right) \times \left[\left(\frac{V_{0,T}}{V_{P,T}} \right)^{\frac{2}{3}} - 1 \right] \right\}$$

In this equation, the thermal dependences of the zero-pressure volume $V_{0,T}$ and bulk modulus $K_{0,T}$ are expressed using the following equations:

$$V_{0,T} = V_{0,300} \times \exp \left[\int_{300}^{T} \alpha_{0,x} dx \right] \tag{3}$$

$$K_{0,T} = K_{0,300} + \left(\frac{\partial K_{0,T}}{\partial T} \right)_P \times (T - 300) \tag{4}$$

where $V_{0,300}$ is the volume at room-*P,T*, and $\alpha_{0,T}$, the thermal expansion, which is empirically assumed to be $\alpha_{0,T} = a_0 + b_0 T$, Eq. (3). $K_{0,T}$ is expressed as a linear function of temperature, its first temperature derivative $(\partial K_{0,T}/\partial T)_P$ and the zero-pressure bulk modulus $K_{0,300}$, Eq. (4). Here we assumed that K'_0 is constant with temperature.

Fitting of our *P–V–T* data with all parameters simultaneously gave the following thermoelastic properties: $K_{0,300} = 163.6 \pm 2.6$ GPa, $K'_0 = 4.1 \pm 0.5$, $V_0 = 1735.9 \pm 0.4$ Å^3, $(\partial K_{0,T}/\partial T)_P = -0.014 \pm 0.004$ GPa K^{-1}, $a_0 = 2.32 \pm 0.13 \times 10^{-5}$ K^{-1}, $b_0 = 2.13 \pm 2.18 \times 10^{-9}$ K^{-2} (e.g., $\alpha_{0,300} = 2.37 \pm 0.20 \times 10^{-5}$ K^{-1}). The bulk modulus $K_{0,300}$ and its pressure derivative determined here are consistent with our fitting of *P–V* data at 300 K. It is also in good agreement with $K_{0,300} = 162$ GPa and $K'_0 = 4.3$, derived from Fan et al.'s (2015) *P–V–T* data. However, we found that their temperature derivative $(\partial K_{0,T}/\partial T)_P = -0.021$ GPa K^{-1} is ~30% smaller than our present value, while their thermal expansion $\alpha_{0,300} = 2.72 \times 10^{-5}$ K^{-1} is about ~15% larger than our $\alpha_{0,300}$ (Table 3), which is in closer agreement with the theoretical value $\alpha_0 = 2.15 \times 10^{-5}$ K^{-1} proposed by Ottonello et al. (1996) based on lattice energy and vibrational energy calculations. The thermal gradient in our cell (see experimental methods) is likely to affect the result of our EoS fitting by ~0.8% for K_T and ~4% for the thermal expansion, but these variations are smaller than the differences between our EoS data and those of Fan et al. (2015), and therefore cannot explain the different thermal parameters for the two studies. Although our room temperatures are in good agreement with those of Fan et al. (2015), our study suggests that unconstrained uncertainties in the data collected at high temperature might still remain between the multi-anvil-apparatus and the diamond-anvil cell, an issue that should be addressed in future experiments.

Fitting of Eqs. (2)–(4) by fixing the first pressure derivative resulted in variations of K_0 and V_0 (Table 3), due to the strong correlation between K_0 and K'. In contrast, the thermal properties $(\partial K_{0,T}/\partial T)_P$ and $\alpha_{0,300}$ did not change in a significant manner, indicating that the thermal proper-

Table 3
Thermoleastic parameters of uvarovite garnet compared to other ugrandite garnets.

|	$V_{0,300}$	$K_{0,300}$ (GPa)	$K'_{0,300}$	$(\partial K_{0,T}/\partial T)_P$ (GPa K^{-1})	$\alpha_{0,300}$ (10^{-5} K^{-1})
Uvarovite					
This study	1735.9 (3)	164.0 (8)	4.0[a]	−0.014 (2)	2.36(17)
	1735.9 (4)	163.6 (26)	4.1 (5)	−0.014 (4)	2.37(20)
	1736.2 (3)	161.5 (8)	4.5[a]	−0.017 (2)	2.45(18)
Fan et al. (2015)	1736.6 (6)	164 (1)	4.0[a]	−0.018 (4)	2.69(12)
	1736.8 (6)	162 (3)	4.3 (4)	−0.021 (4)	2.72(14)
	1737.0 (6)	161 (1)	4.5[a]	−0.022 (4)	2.76(13)
This study + Fan et al. (2015)	1736.7 (6)	161.0 (28)	4.5 (4)	−0.018 (3)	2.63(11)
Grossular					
Milman et al. (2001)	1667	166	4.3	–	–
Gréaux et al. (2010)	1664[a]	166[a]	4.0 (1)	−0.019 (1)	2.74(23)
Gwanmesia et al. (2013)	1662.1 (3)	169.7 (8)	4.47 (1)	–	–
Andradite					
Milman et al. (2001)	1753.2	147	4.4	–	–
Pavese et al. (2001)	1753.9 (5)	158 (2)	4.0[a]	−0.017 (9)	3.17(6)
Jiang et al. (2004)	–	154.5 (6)	4.7 (1)	–	–
Goldmanite					
Milman et al. (2001)	1762.8	139	4.7	–	–

[a] Fixed during fitting.
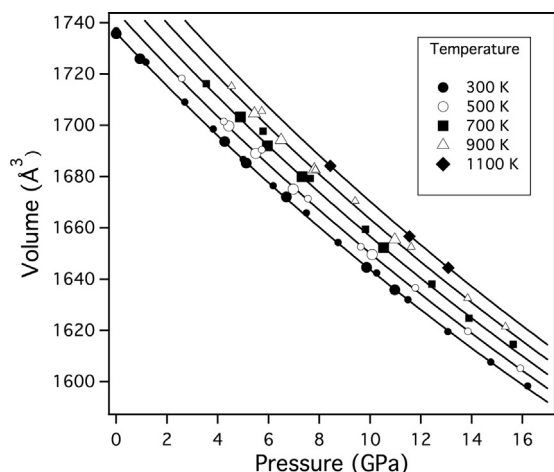
Fig. 4. Unit-cell volume of uvarovite garnet as a function of pressure and temperature. Data at 300 K (plain circle), 500 K (open circle), 700 K (plain square), 900 K (open triangle), and 1100 K (plain diamond) are represented respectively. Large symbols represent our data, while small symbols are from Fan et al. (2015). For all our data, pressure and volume error bars are within the size of the symbols. Solid lines represent the isothermal compression curves obtained from fitting all the data to a Birch–Murnaghan EoS.

ties of uvarovite are either less affected or unaffected by the variation of the bulk modulus and of its pressure derivative. A similar conclusion was reached by other experimental studies on the elasticity of silicate garnets (Fan et al., 2015; Gréaux and Yamada, 2013; Zou et al., 2012a). Fitting of all available data from our study and that of Fan et al. (2015) gave the following parameters: $K_{0,300} = 161.0 \pm 2.8$ GPa, $K'_0 = 4.5 \pm 0.4$, $V_0 = 1736.7 \pm 0.6$ Å^3, $(\partial K_{0,T}/\partial T)_P = -0.018 \pm 0.003$ GPa K^{-1}, $\alpha_{0,300} = 2.63 \pm 0.11 \times 10^{-5}$ K^{-1} (Fig. 4). The temperature derivative of the bulk modulus $(\partial K_{0,T}/\partial T)_P$ is similar to those of grossular and andradite in previous studies (Gréaux et al., 2010; Pavese et al., 2001), suggesting that the values of $(\partial K_{0,T}/\partial T)_P$ of ugrandite garnets are independent of the 3+ cations in the garnet octahedral site. The thermal expansion coefficient $\alpha_0 = 2.40$–2.53×10^{-5} K^{-1} is smaller than that of grossular (Gréaux et al., 2010) and andradite (Pavese et al., 2001), although the difference between uvarovite and grossular fall within their respective uncertainties. Besides, the higher value proposed for andradite could have resulted from the use of a different expression for the thermal parameters in the EoS as Pavese et al. (2001) expressed $\alpha = $ cste instead of $\alpha = a_0 + b_0T$ used in the present study and Gréaux et al. (2010).

4. Discussion

4.1. Comparison with other garnets of the ugrandite group

The ugrandite is a family of isostructural garnets with the formula $Ca_3Y_2Si_3O_{12}$, where the Y-site is commonly occupied either by Al (grossular), Fe (andradite), Cr (uvarovite), or V (goldmanite). The bulk moduli $K_0 = 162$–165 GPa determined in this study showed that the compressibility of uvarovite is in between that of andradite ($K_0 = 154$–158 GPa) (Jiang et al., 2004; Pavese

et al., 2001) and grossular ($K_0 = 166$–171.5 GPa) (Gréaux et al., 2010; Gwanmesia et al., 2013), although differences in K_0 depend on the value of K' adopted in the respective studies. In their study, Fan et al. (2015) neglected this aspect when they proposed representing the bulk modulus of ugrandite garnet as a linear function of the unit-cell volume. The validity of such a relation can be tested by using the derived elastic properties to calculate the compression curve of a garnet solid solution and comparing the result to actual data.

Fig. 5 shows the calculated densities of a grossular/ uvarovite solid solution compared with the experimental study of Diella et al. (2004), who reported the compressibility of a natural garnet sample containing ∼62 mol% of uvarovite using a diamond-anvil cell and synchrotron X-ray diffraction. The density of the garnet solid solution was estimated from a weighted summation of the individual elastic properties of the corresponding end members (e.g., Pamato et al., 2016). In this approach we assumed that elastic properties vary linearly as a function of the endmember proportions in the solid solution. The calculated densities are in relatively good agreement with experimental data, while both experimental and theoretical datasets stand in between the densities of the uvarovite (this study) and grossular (Gréaux et al., 2010) endmembers. The experimental densities of Diella et al. (2004) are generally smaller than those of uvarovite (Fig. 3), which can be explained by the smaller unit-cell volume of grossular (∼1662–1664 Å^3) compared to that of uvarovite (∼1727–1738 Å^3). We noted, however, that when using garnet endmember proportions as given by their electron
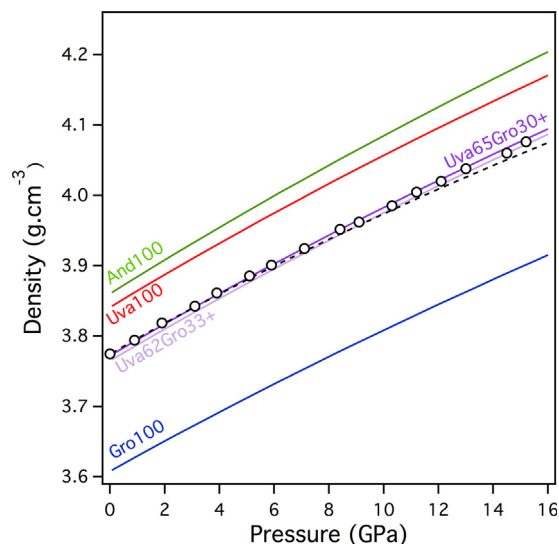

Fig. 5. Experimental and calculated densities of natural uvarovite-rich garnet. Open circles represent the experimental data of Diella et al. (2004), while the purple solid lines represent our calculated densities for the composition 62% uvarovite, 33% grossular, 5% spessartine and 1% andradite (Uva62Gro33+, light purple) and 65% uvarovite, 30% grossular, 2% pyrope, 1% almandine, 1% spessartine, and 1% andradite (Uva65Gro30+, dark purple). The broken line represents the same calculation for Uva65Gro30+ using the elastic parameters of Fan et al. (2015). The density curve of grossular (blue line), uvarovite (red line) and andradite (green line) ugrandite garnet endmembers are shown for comparison.

probe analyses (Fig. 5, Uv62Gr33+), the calculated densities are slightly lower than the experimental data. Instead, we found a better agreement between the weighted average and experimental data (Diella et al., 2004) when we used the endmember proportions (in mol%): 65% uvarovite, 30% grossular, 2% pyrope, 1% almandine, 1% spessartine, and 1% andradite (Fig. 5, Uv65Gr30+). The amount of uvarovite that we propose here is slightly higher than the value measured with an electron probe; this difference could be derived from unconstrained uncertainties in our respective experiments. On the other hand, we can see in Fig. 5 that density calculated using Fan et al.'s (2015) linear model fits well with Diella et al.'s (2004) data at low pressure, but fails to explain densities at pressures higher than ∼5 GPa, which is likely due to their higher K' values, as discussed above.

Such features could be explained based on the crystal structure of silicate garnets. The cubic garnet structure consists of large dodecahedral sites, which share edges with corner-linked chains of alternating SiO_4 tetrahedra and YO_6 octahedra, and with each other (Novak, 1971). Previous theoretical studies have demonstrated that the size of the dodecahedral cation likely controls the variations in the elasticity of silicate garnets with Al and Si in the octahedral site (Milman et al., 2000; Pacalo et al., 1992). However, there is no firm explanation for the lower values observed for garnets with transition metals in the octahedral site such as andradite and uvarovite garnets. In addition, the dodecahedral cavity of ugrandite garnet is filled with a large Ca^{2+} cation, so the rotational freedom within the corner-linked chains is limited, resulting in the structure becoming more rigid compared to other garnet groups (Milman et al., 2000; Pacalo et al., 1992). Based on the similarities in site occupancies, it is therefore likely that the characteristics of the trivalent cation and the resulting compressibility of the octahedral site might play a major role in controlling the variations of elasticity between ugrandite garnets. Our results go in that direction, showing that ugrandite garnets with a small octahedral site (e.g., grossular) have higher bulk modulus than garnets with a larger octahedral site (e.g., uvarovite, andradite). It is compatible with former studies in pyroxenes, olivines, and spinels, which showed that transition metals in octahedral coordination tend to decrease the elastic moduli of those minerals (Bass and Weidner, 1984; Pacalo et al., 1992; Zhang et al., 1998). Our results also suggest that ugrandite garnet with transition metals in the octahedral site (e.g., uvarovite, andradite) might become more incompressible upon increasing pressure, hence yielding higher K' than garnet with Al in the octahedral site. It is, however, difficult to come to a firm conclusion about the K' value of silicate garnets, as experimental values generally fall between 4 and 5 (Gwanmesia et al., 2006; Kono et al., 2010; Zou et al., 2012b) with differences between species barely standing outside of their respective uncertainties.

4.2. Implications for the density of the upper mantle

Petrological studies of minerals in kimberlite and alkali basalts that returned from the deep mantle revealed that the upper mantle is largely constituted of aluminous lherzolite. It is also known that lherzolite undergoes an important transition from spinel lherzolite to garnet lherzolite at high pressures between ∼2 GPa and ∼7 GPa, which strongly depends on the Cr/(Cr + Al) ratio of the system (Klemme, 2004). In this reaction, Cr and Ca increasingly substitute into the garnet with increasing pressure, resulting in an increase in the grossular and uvarovite components of mantle garnets. Using our elasticity data on uvarovite, combined with those of other garnet endmembers, we estimated the density variation in garnet lherzolite as a function of depth along an average mantle geotherm. Here we postulated that Cr is only present through the uvarovite endmember, assuming that the knorringite component may be minor at the pressures and temperatures of the upper mantle, although its proportions might increase with increasing pressure (Zou and Irifune, 2012). Either way, it is difficult to implement this parameter in our model, as the precise thermoelastic data of pure knorringite garnet are unavailable to this day.

Fig. 6 shows the calculated density profiles of simplified mantle garnets with the following compositions: 75% pyrope and 25% grossular (Py75Gr25), and 75% pyrope and 25% uvarovite (Py75Uva25), compared to those of pyrope, which is the major component of upper-mantle garnets. It is interesting to note that densities of Py75Gr25 are only ∼0.5% higher than those of pyrope, suggesting that mantle garnet may not be sensitive to variations of the grossular component; e.g., Cr/(Cr + Al) = 0. In contrast, we found a more substantial ∼2% density increase when incorporating the uvarovite component (Py75Uva25); e.g., Cr/(Cr + Al) = 1. Garnet compositions in lherzolite xenoliths from alkali basalts and kimberlites generally yield a Cr/(Cr + Al) < 0.2–0.35 (Grutter et al., 2006), which would
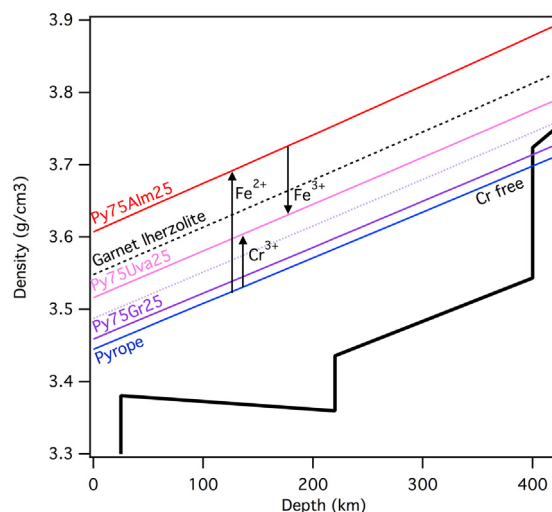

Fig. 6. Model densities of mantle garnet solid solutions as a function of depth. The blue line represents densities of pyrope (i.e. Cr-free) from what we increased grossular (Py75Gr25, purple line), uvarovite (Py75Uva25, pink line) and almandine (Py75Alm25, red line) proportions respectively. The broken line represents the calculated density of a lherzolite garnet based on the chemical analyses of a fertile peridotite garnet brought up by alkali basalts (McDonough and Rudnick, 1998), which yielded the following composition: 75% pyrope, 13% almandine, 9% pyrope, 4% uvarovite, and 1% andradite.

correspond to a ∼1% density increase compared to the pyrope endmember. Higher Cr/(Cr + Al) ratios > 0.5 are reported in chromite-saturated harzburgite garnets, but those compositions are Ca-depleted, implying the formation of a knorringite-rich pyrope garnet, for which our model is non-applicable. It should also be mentioned that lherzolite garnets bear a substantial amount of Fe, although its exact chemical behavior is not well known. If we consider only Fe^{2+} as the main garnet species (Py75Alm25, Fig. 6), density increases drastically due to the high density of the almandine endmember. In contrast, the presence of Fe^{3+} would decrease density compared to Py75Alm25 due to the lower density of the andradite endmember, which is almost the same as that of uvarovite. However, the increase of andradite garnet along with the presence of Fe^{3+} would be incompatible with the relatively low Ca contents of garnet lherzolite (McDonough and Rudnick, 1998), suggesting that Fe^{2+} might be the main species in natural systems. Fig. 6 shows that high Fe^{2+} content is more likely to affect the bulk density of mantle garnet rather than the incorporation of Cr^{3+}. However, because Cr^{3+} and Fe^{3+} are positively correlated in upper mantle garnets (e.g., Canil and O'Neill, 1996; Nimis et al., 2015), the presence of the Cr-rich component might also favor the formation of Fe^{3+}, hence resulting in a decrease of the mantle garnet density. Our results emphasize that the mantle garnet density could vary substantially upon Cr/(Cr + Al) increase, which seems to occur at upper mantle depths, as Cr-rich garnets are commonly found in diamond inclusions.

The density of a natural garnet lherzolite was estimated based on the elasticity of garnet endmembers and the chemical analyses of a fertile peridotite garnet brought up by alkali basalts (McDonough and Rudnick, 1998); it yielded the following: 75% pyrope, 13% almandine, 9% grossular, 4% uvarovite and 1% andradite. Our estimates show that the density of garnet lherzolite would be ∼2.5% higher compared to the Cr- and Fe-free Py75Gr25 garnet (Fig. 6), which may have some implications for the seismic discontinuity at depths of 50–100 km. This discontinuity has been observed globally, but the depth is not the same everywhere (Hales, 1969; Yamasaki and Nakada, 1997); a difference that is attributed to the shift of the spinel-garnet phase boundary from ∼2 GPa in Al-rich fertile mantle compositions to ∼7 GPa in the deeper continental crust (Klemme, 2004; Klemme and O'Neill, 2000), where Al is depleted and Cr and Fe are more abundant, as a possible consequence of melting events (Walter et al., 2002). The higher density of Cr- and Fe-rich garnets further emphasizes the importance of the spinel-garnet transition and offers an alternative to thermal anomalies in order to explain the increase in seismic velocity at depths of ∼100 km (Hales, 1969; Yamasaki and Nakada, 1997). These conclusions, however, would need to be completed by the contribution of the knorringite garnet endmember, which is likely to change such behavior at higher pressure and high Cr/(Cr + Al) ratios.

5. Conclusion

In the present study, we investigated the elasticity of uvarovite garnet as a function of pressure and temperature up to 13 GPa and 1100 K, using the multi-anvil apparatus combined with *in situ* synchrotron X-ray diffraction. The results are generally in good agreement with a recent study that used the laser heated diamond anvil cell up to 16 GPa and 900 K, although our results suggest slightly milder pressure and temperature dependences of the bulk modulus. The present data are compatible with the compressibility of grossular/uvarovite specimens, such as what is found in natural systems. The present results highlight the effect of 3+ cations substitution on the thermoelasticity of garnets and call for more systematic studies on other ugrandite end-members (e.g., andradite, goldmanite) at simultaneous high pressure and high temperature. Based on a comparison with the elasticity of other garnet endmembers, we proposed that the incorporation of Cr^{3+} and Fe^{3+} in the Y-site of the garnet structure is likely to increase the density of ugrandite garnets, resulting in a substantial increase of density in regions where Cr-rich spinel releases chromium in the garnet through metasomatic reactions. Further constraints on the other silicate garnet end-members at high pressure and high temperature will be particularly valuable to understand the behavior of mantle garnets at high *P* and *T*, since they usually display relatively complex compositions in a natural environment.

References

Andrut, M., Wildner, M., 2002. The crystal chemistry of birefringent natural uvarovites. Part III. Application of the superposition model of crystal fields with a characterization of synthetic cubic uvarovite. Phys. Chem. Miner. 29, 595–608, http://dx.doi.org/10.1007/s00269-002-0264-4.

Angel, R.J., 2000. Equations of State. Rev. Mineral. Geochem. 41, 35–59, http://dx.doi.org/10.2138/rmg.2000.41.2.

Bass, J.D., 1986. Elasticity of uvarovite and andradite garnets. J. Geophys. Res. 91, 7505–7516, http://dx.doi.org/10.1029/JB091iB07p07505.

Bass, J.D., 1989. Elasticity of grossular and spessartite garnets by Brillouin spectroscopy. J. Geophys. Res. 94, 7621–7628.

Bass, J.D., Anderson, D.L., 1984. Composition of the upper mantle: geophysical tests of two petrological models. Geophys. Res. Lett. 11, 229–232.

Bass, J.D., Weidner, D.J., 1984. Elasticity of single-crystal orthoferrosilite. J. Geophys. Res. 89 (B6), 4359–4371.

Canil, D., O'Neill, H.S.C., 1996. Distribution of Ferric Iron in some Upper-Mantle Assemblages. J. Petrol. 37, 609–635, http://dx.doi.org/10.1093/petrology/37.3.609.

Challis, G.A., Grapes, R., Palmer, K., 1995. Chromian muscovite, uvarovite, and zincian chromite; products of regional metasomatism in North-west Nelson, New Zealand. Can. Mineral. 33, 1263–1284.

Conrad, P.G., Zha, C.S., Mao, H·K., Hemley, R.J., 1999. The high-pressure, single-crystal elasticity of pyrope, grossular, and andradite. Am. Mineral. 84, 374–383.

Deer, W.A., Howie, R.A., Zussman, J., 1962. Rock-forming Minerals. Longmans, London.

Diella, V., Sani, A., Levy, D., Pavese, A., 2004. High-pressure synchrotron X-ray diffraction study of spessartine and uvarovite: a comparison

between different equation of state models. Am. Mineral. 89, 371–376.

Fan, D., Xu, J., Ma, M., Wei, S., Zhang, B., Liu, J., 2015. PVT equation of state of $Ca_3Cr_2Si_3O_{12}$ uvarovite garnet by using a diamond-anvil cell and in-situ synchrotron X-ray diffraction. Am. Mineral. 100, 588–597, http://dx.doi.org/10.2138/am-2015-5002.

Gréaux, S., Yamada, A., 2013. P–V–T equation of state of $Mn_3Al_2Si_3O_{12}$ spessartine garnet. Phys. Chem. Miner. 41, 141–149, http://dx.doi.org/10.1007/s00269-013-0632-2.

Gréaux, S., Kono, Y., Nishiyama, N., Kunimoto, T., Wada, K., Irifune, T., 2010. P–V–T equation of state of $Ca_3Al_2Si_3O_{12}$ grossular garnet. Phys. Chem. Miner. 38, 85–94, http://dx.doi.org/10.1007/s00269-010-0384-1.

Green, D.H., Ringwood, A.E., 1967. The stability fields of aluminous pyroxene peridotite and garnet peridotite and their relevance in upper mantle structure. Earth Planet. Sci. Lett. 3, 151–160.

Grutter, H., Latti, D., Menzies, A., 2006. Cr-saturation arrays in concentrate garnet compositions from kimberlite and their use in mantle barometry. J. Petrol. 47 (4), 801–820, http://dx.doi.org/10.1093/petrology/egi096.

Gwanmesia, G.D., Wang, L., Heady, A., Liebermann, R.C., 2013. Elasticity and sound velocities of polycrystalline grossular garnet (Ca_3Al_2 Si_3O_{12}) at simultaneous high pressures and high temperatures. Phys. Earth Planet. Inter. 228, 1–8, http://dx.doi.org/10.1016/j.pepi.2013.09.010.

Gwanmesia, G.D., Zhang, J., Darling, K., Kung, J., Li, B., Wang, L., Neuville, D., Liebermann, R.C., 2006. Elasticity of polycrystalline pyrope ($Mg_3Al_2Si_3O_{12}$) to 9 GPa and 1000 °C. Phys. Earth Planet. Inter. 155, 179–190, http://dx.doi.org/10.1016/j.pepi.2005.10.008.

Hales, A.L., 1969. A seismic discontinuity in the lithosphere. Earth Planet. Sci. Lett. 7, 44–46.

Irifune, T., Ohtani, E., Kumazawa, M., 1982. Stability field of knorringite $Mg_3Cr_2Si_3O_{12}$ at high pressure and its implication to the occurrence of Cr-rich pyrope in the upper mantle. Phys. Earth Planet. Inter. 27, 263–272.

Jiang, F., Speziale, S., Shieh, S.R., Duffy, T.S., 2004. Single-crystal elasticity of andradite garnet to 11 GPa. J. Phys. Condens. Matter 16, S1041–S1052, http://dx.doi.org/10.1088/0953-8984/16/14/014.

Klemme, S., 2004. The influence of Cr on the garnet–spinel transition in the Earth's mantle: experiments in the system $MgO–Cr_2O_3–SiO_2$ and thermodynamic modelling. Lithos 77, 639–646, http://dx.doi.org/10.1016/j.lithos.2004.03.017.

Klemme, S., O'Neill, H.S., 2000. The near-solidus transition from garnet lherzolite to spinel lherzolite. Contrib. Mineral. Petrol. 138, 237–248, http://dx.doi.org/10.1007/s004100050560.

Kono, Y., Gréaux, S., Higo, Y., Ohfuji, H., Irifune, T., 2010. Pressure and temperature dependences of elastic properties of grossular garnet up to 17 GPa and 1 650 K. J. Earth Sci. 21, 782–791.

Léger, J.-M., Redon, A.M., Chateau, C., 1990. Compressions of synthetic pyrope, spessartine and uvarovite garnets up to 25 GPa. Phys. Chem. Miner. 17, 161–167, http://dx.doi.org/10.1007/BF00199668.

McDonough, W.F., Rudnick, R.L., 1998. Mineralogy and composition of the upper mantle. Rev. Mineral. 37, 139–164 (Incomplete reference).

Milman, V., Akhmatskaya, E.V., Nobes, R.H., Winkler, B., Pickard, C.J., White, J.A., 2001. Systematic ab initio study of the compressibility of silicate garnets. Acta Crystallogr. Sect. B-Struct. Commun. 57, 163–177, http://dx.doi.org/10.1107/S0108768100018188.

Milman, V., Winkler, B., Nobes, R.H., Akhmatskaya, E.V., Pickard, C.J., White, J.A., 2000. Garnets: structure, compressibility, dynamics, and disorder. JOM 52, 22–25, http://dx.doi.org/10.1007/s11837-000-0156-3.

Mogessie, A., Rammlmair, D., 1994. Occurrence of zoned uvarovite-grossular garnet in a rodingite from the Vumba Schist Belt, Botswana, Africa: implications for the origin of rodingites. Mineral. Mag. 58, 375–386 (Incomplete reference).

Nimis, P., Goncharov, A., Ionov, D.A., McCammon, C., 2015. Fe^{3+} partitioning systematics between orthopyroxene and garnet in mantle peridotite xenoliths and implications for thermobarometry of oxidized and reduced mantle rocks. Contrib. Mineral. Petrol. 169, 14–19, http://dx.doi.org/10.1007/s00410-014-1101-8.

Nishiyama, N., Wang, Y., Sanehira, T., Irifune, T., Rivers, M., 2008. Development of the Multi-anvil Assembly 6-6 for DIA and D-DIA type high-pressure apparatuses. High Pressure Res. 28, 307–314, http://dx.doi.org/10.1080/08957950802250607.

Novak, G.A., 1971. The Crystal Chemistry of the Silicate Garnets. Am. Mineral. 56, 122.

Novak, G.A., Gibbs, G.V., 1971. The crystal chemistry of the silicate garnets. Am. Mineral. 56, 791–825.

Ottonello, G., Bokreta, M., Sciuto, P.F., 1996. Parameterization of energy and interactions in garnets; end-member properties. Am. Mineral. 81, 429–447.

Pacalo, R., Weidner, D.J., Gasparik, T., 1992. Elastic properties of sodium-rich majorite garnet. Geophys. Res. 19, 1895–1898.

Pamato, M.G., Kurnosov, A., Ballaran, T.B., Frost, D.J., Ziberna, L., Giannini, M., Speziale, S., Tkachev, S.N., Zhuravlev, K·K., Prakapenka, V.B., 2016. Single crystal elasticity of majoritic garnets: Stagnant slabs and thermal anomalies at the base of the transition zone. Earth Planet. Sci. Lett. 451, 114–124, http://dx.doi.org/10.1016/j.epsl.2016.07.019.

Pavese, A., Diella, V., Pischedda, V., Merli, M., Bocchio, R., Mezouar, M., 2001. Pressure-volume-temperature equation of state of andradite and grossular, by high-pressure and -temperature powder diffraction. Phys. Chem. Miner. 28, 242–248, http://dx.doi.org/10.1007/s002690000144.

Proenza, J., Solé, J., Melgarejo, J.C., 1999. Uvarovite in podiform chromitite: the Moa-Baracoa ophiolitic massif. Cuba. Can. Mineralogist. 37 (3), 679–690.

Seto, Y., Nishio-Hamane, D., Nagai, T., Sata, N., 2010. Development of a Software Suite on X-ray Diffraction Experiments. Rev. High Pressure Sci. Technol. 20, 269–276, http://dx.doi.org/10.4131/jshpreview.20.269.

Sinogeikin, S.V., Bass, J.D., 2002. Elasticity of majorite and a majorite-pyrope solid solution to high pressure: implications for the transition zone. Geophys. Res. Lett. 29 (2), 1017, http://dx.doi.org/10.1029/2001GL013937.

Tange, Y., Nishihara, Y., Tsuchiya, T., 2009. Unified analyses for P–V–T equation of state of MgO: a solution for pressure-scale problems in high-P–T experiments. J. Geophys. Res. B Solid Earth 114 (3.) .

Tsuchiya, T., 2003. First-principles prediction of the P–V–T equation of state of gold and the 660-km discontinuity in Earth's mantle. J. Geophys. Res. B Solid Earth 108.

Walter, M., Katsura, T., Kubo, A., Shinmei, T., Nishikawa, O., Ito, E., Lesher, C., Funakoshi, K., 2002. Spinel–garnet lherzolite transition in the system $CaO–MgO–Al_2O_3–SiO_2$ revisited: an in situ X-ray study. Geochim. Cosmochim. Acta 66, 2109–2121, http://dx.doi.org/10.1016/s0016-7037(02)00845-1.

Wang, Z., Ji, S., 2001. Elasticity of six polycrystalline silicate garnets at pressure up to 3.0 GPa. Am. Mineral. 86, 1209–1218.

Yamasaki, T., Nakada, M., 1997. The effects of the spinel-garnet phase transition on the formation of rifted sedimentary basins. Geophys. J. Int. 130, 681–692, http://dx.doi.org/10.1111/j.1365-246x.1997.tb01862.x.

Zhang, L., Ahsbahs, H., Kutoglu, A., 1998. Hydrostatic compression and crystal structure of pyrope to 33 GPa. Phys. Chem. Miner. 25 (4), 301–307.

Zou, Y., Gréaux, S., Irifune, T., Whitaker, M.L., Shinmei, T., Higo, Y., 2012a. Thermal equation of state of $Mg_3Al_2Si_3O_{12}$ pyrope garnet up to 19 GPa and 1700 K. Phys. Chem. Miner. 39, 589–598, http://dx.doi.org/10.1007/s00269-012-0514-z.

Zou, Y., Irifune, T., 2012. Phase relations in $Mg_3Cr_2Si_3O_{12}$ and formation of majoritic knorringite garnet at high pressure and high temperature. J. Mineral. Petrol. Sci. 107, 197–205.

Zou, Y., Irifune, T., Gréaux, S., Whitaker, M.L., Shinmei, T., Ohfuji, H., Negishi, R., Higo, Y., 2012b. Elasticity and sound velocities of polycrystalline $Mg_3Al_2(SiO_4)_3$ garnet up to 20 GPa and 1700 K. J. Appl. Phys. 112, 014910, http://dx.doi.org/10.1063/1.4736407.